Feature Article

Current Status of the Synchrotron Small-Angle X-ray Scattering Station BL4C1 at the Pohang Accelerator Laboratory

Jörg Bolze, Jehan Kim, Jung-Yun Huang, Seungyu Rah, and Hwa Shik Youn*

Pohang Accelerator Laboratory, Pohang University of Science and Technology,
San 31, Hyoja-dong, Pohang 790-784, Korea

Byeongdu Lee, Tae Joo Shin, and Moonhor Ree*

Dept. of Chemistry, Center for Integrated Molecular Systems, BK21 Functional Polymer Thin Film Group,
and Polymer Research Institute, Pohang University of Science and Technology,
San 31, Hyoja-dong, Pohang 790-784, Korea

Abstract : The small-angle X-ray scattering (SAXS) beamline BL4C1 at the 2.5 GeV storage ring of the Pohang Accelerator Laboratory (PAL) has been in its first year of operation since August 2000. During this first stage it could meet the basic requirements of the rapidly growing domestic SAXS user community, which has been carrying out measurements mainly on various polymer systems. The X-ray source is a bending magnet which produces white radiation with a critical energy of 5.5 keV. A synthetic double multilayer monochromator selects quasi-monochromatic radiation with a bandwidth of ca. 1.5%. This relatively low degree of monochromatization is sufficient for most SAXS measurements and allows a considerably higher flux at the sample as compared to monochromators using single crystals. Higher harmonics from the monochromator are rejected by reflection from a flat mirror, and a slit system is installed for collimation. A charge-coupled device (CCD) system, two one-dimensional photodiode arrays (PDA) and imaging plates (IP) are available as detectors. The overall performance of the beamline optics and of the detector systems has been checked using various standard samples. While the CCD and PDA detectors are well-suited for diffraction measurements, they give unsatisfactory data from weakly scattering samples, due to their high intrinsic noise. By using the IP system smooth scattering curves could be obtained in a wide dynamic range. In the second stage, starting from August 2001, the beamline will be upgraded with additional slits, focusing optics and gas-filled proportional detectors.

Keywords : synchrotron X-ray, small-angle X-ray scattering, beamline.

Introduction

Small-angle X-ray scattering from an irradiated specimen arises from electron density fluctuations on a mesoscopic length scale in the range of ca. 10 to 500 Å. This method has become a very important tool for structural studies on a wide variety of materials, such as polymers, fibers, metals and alloys, liquid crystals, and colloidal systems.[1-5] Examples for colloids which have been investigated are biomolecules,[6] synthetic nanoparticles, aggregates of amphiphilic molecules, gels etc. Information about the overall shape and size of the scattering object, its density, orientation, packing with other objects etc. may be obtained. Typical applications in poly-

mer science[7,8] are studies on the nanodomain formation in block copolymer systems as a function of temperature and composition, on the crystallization mechanisms and kinetics of homo-polymers and copolymers, on the structure of polymer latexes, on the conformation of polymers in solution etc. Due to the high photon flux which is available at synchrotron sources, the data collection times can be greatly reduced which also allows for time-resolved studies on phase transitions, crystallization kinetics, assembly/disassembly processes, denaturation/renaturation etc. Other merits of synchrotron radiation are the naturally low beam divergence and the available wavelength continuum.

Beamline BL4C1 at the Pohang Accelerator Laboratory (PAL)[9,10] is the first dedicated synchrotron small-angle X-ray scattering station in Korea. The first phase of construction was started in January 1999 and completed in August 2000.

Domestic SAXS user and SAXS working groups were founded in 1994 and 1995, respectively, and have been growing rapidly. To date, simple optical components have been installed at the beamline, which can meet the basic requirements of the domestic SAXS community. This paper summarizes the current status of the beamline instrumentation and reports about some measurements on standard samples, which were conducted to test the performance of the beamline optics and of the various detector systems. A brief outlook on to further upgrading plans is also given.

Source

The Pohang Accelerator Laboratory (PAL) is a 2.5 GeV synchrotron radiation facility in Pohang, Korea. It is operated at a ring current of typically 150-200 mA. The radiation source for the SAXS beamline is a bending magnet with a magnetic field of 1.32 T. The size of the source (root mean square deviation σ of the electron beam with respect to the orbit) is $\sigma_v = 0.059$ mm vertically and $\sigma_h = 0.160$ mm horizontally, and the divergence of the emitted white beam is 0.1 mrad vertically and 3.0 mrad horizontally. At a stored electron energy of 2.5 GeV the critical energy of radiation is 5.5 keV and a usable photon flux up to 15 keV is delivered. The calculated angular photon flux density (which is given in units of the number of photons per unit time (s), per unit solid angle (mrad^2), and per 0.1% relative bandwidth) amounts to 2.15×10^{13} photons/s/mrad^2/0.1% b.w. at a stored electron energy of 2.5 GeV, a ring current of 200 mA and an energy of radiation of 7.7 keV. The ultra-high vacuum in the storage ring is separated from the high vacuum beamline by a beryllium window. The access of the X-ray beam to the experimental station is controlled by a photon shutter.

Beamline Optics

Monochromator. The monochromator is located at a distance of 15 m from the source of radiation. It consists of a set of two synthetic multilayers (Osmic Inc.) which are deposited on silicon substrates with a size of $20 \times 50 \times 5$ mm. Each multilayer consists of 200 W/B$_4$C layers, with a d-spacing of 25 ± 1 Å and a root-mean-square roughness smaller than 1 Å. The first order Bragg reflection of these multilayers is used to obtain a quasi-monochromatic beam. The reflectivity at the Bragg angle amounts to ca. 70% at 8 keV and the band width of the reflected beam, which is mainly determined by the number of layers, is ca. 1.5%. In addition to the fundamental, the second harmonic is also present in the same reflected beam. As will be described further below, it is removed downstream using the reflection from a flat mirror. The two multilayers are mounted on a holder in a parallel geometry and offset the incoming beam ca. 3 mm upwards without changing its direction. This optical system yields X-rays with energies E varying from 7.5 to 9.5 keV. The beamline is usually operated at $E = 7.709$ keV, which corresponds to a wavelength λ of 1.607 Å. Energy calibration is done using the K-absorption edge of a cobalt foil. At that energy the Bragg angle of the multilayer is 1.842° and the vertical beam size which is intercepted by the monochromator is 1.6 mm. The resolution of the double multilayer monochromator in terms of $\Delta\lambda/\lambda$, where $\Delta\lambda$ represents the full width at half maximum of the reflected wavelength distribution, is ca. 1.5%. This degree of monochromatization is rather poor compared to that of single crystal monochromators, for which $\Delta\lambda/\lambda$, is of the order of 10^{-4}. The advantage of a wide-bandpass monochromator as being used here, however, is a considerable gain of photon flux by about a factor of 100.

In the following we discuss how the monochromator characteristics will affect scattering and di-ffraction data. A wavelength spread in the radiation incident on a specimen leads to a distribution of scattering vectors q ($q = 4\pi \times \sin (\theta/2)/\lambda$, where θ denotes the scattering angle) which are being probed simultaneously at one angle in the detector plane. The scattering curve $\tilde{I}(q)$, which is measured from a sample when using a polychromatic beam with a wave-
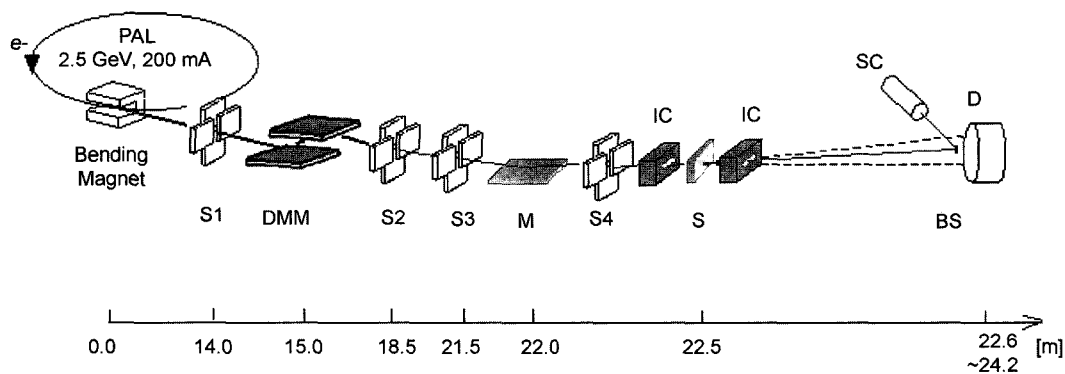

Figure 1. Schematic diagram of the SAXS beamline BL4C1 at the Pohang Accelerator Laboratory: S1-S4: slits; DMM: double mulitlayer monochromator; M: flat mirror; S: sample; IC: ionization chamber; BS: beamstop; SC: scintillation counter; D: detector.

length distribution $W(\lambda')$, is related to the scattering pattern $I(q)$, which would be measured in case of an ideally monochromatic beam ($\Delta\lambda/\lambda = 0$), by the following smearing integral:[2]

$$\tilde{I}(q) = \int_0^\infty W(\lambda') \cdot I\left(\frac{q}{\lambda'}\right) d\lambda' \qquad (1)$$

where $\lambda' = \lambda/\lambda_0$ and λ_0 denotes the mean wavelength. From this equation, it can be seen that there is no smearing effect at $q = 0$ nm^{-1}, and that the width of distribution in q, over which $I(q)$ is being averaged, increases with q. In order to estimate the smearing effect due to the finite energy resolution of the monochromator used at BL4C1, a computer program was written, which applies the smearing integral given in equation (1) to various calculated model scattering patterns.

First we discuss the scattering from an assembly of non-interacting, homogeneous spheres with a mean sphere diameter of 100 nm. A Gaussian particle size distribution with a rather small standard deviation of 3% was assumed. This kind of model system may represent a dilute polymer dispersion (latex). The scheme for calculating the scattering intensity of such a system was reported elsewhere.[11] Figure 2 displays the scattering patterns which were calculated as a function of $\Delta\lambda/\lambda$, where $W(\lambda')$ was assumed to be a Gaussian. The model curve calculated for the case of an ideally monochromatic beam exhibits deep minima in the oscillations because symmetric particles with a narrow particle size distribution are being considered. In case of $\Delta\lambda/\lambda = 1.5\%$, no significant smearing of the oscillations occurs, whereas in case of $\Delta\lambda/\lambda = 10\%$ (a typical resolution for neutron scattering) considerable smearing is evident. Thus, such a sample can be measured using the double multilayer monochromator at BL4C1, without any drawback in resolution. On the other hand, if the data were measured with a resolution of $\Delta\lambda/\lambda = 10\%$, a desmearing of the scattering curve would be necessary. Otherwise, the determination of the particle size polydispersity would lead to an erroneous result.

Next we consider the diffraction from a sample containing some ordered domains. The Bragg peak originating from this sample is assumed to be Gaussian with an intrinsic line width (standard deviation) of $\sigma = 0.0500$ nm^{-1}. This corresponds to a correlation length of 54 nm in real space. In Figure 3 it is shown how the width of the Bragg peak is affected by a finite energy resolution of 1.5%. In order to elucidate how the smearing effect depends on the diffraction angle, various d-spacings were assumed. It can be seen, that significant peak broadening is induced, and that the effect increases considerably with increasing scattering vector. As an example, the peak width is broadened by 3.2% at $q =$ 2 nm^{-1} (SAXS regime), but at $q = 10$ nm^{-1} (WAXD regime) by as much as 62%. Before any quantitative interpretation of such data is done, a desmearing of the raw data is required.
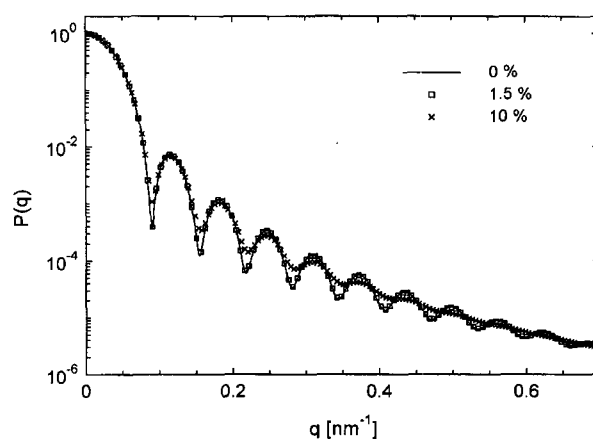

Figure 2. Model calculation demonstrating how SAXS data are affected by a finite wavelength resolution of the monochromator. Shown is the form factor $P(q)$ of a homogenous sphere with a radius of 50 nm. The standard deviation of the Gaussian particle size distribution was set to 1.5 nm or 3%. Parameter is the width of the wavelength distribution in the incident X-ray beam which is assumed to be Gaussian. The smearing effect due to a bandwidth $\Delta\lambda/\lambda$ of 1.5% (as provided by the double multilayer monochromator) is still negligible, whereas 10% bandwidth would result in a considerable smearing of the extrema.
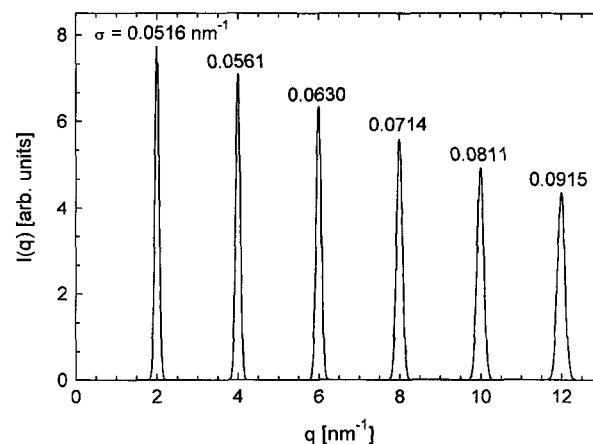

Figure 3. Model calculation demonstrating how the width of a diffraction peak is affected by a finite wavelength resolution of the monochromator. The wavelength distribution in the incident beam was assumed to be Gaussian with $\Delta\lambda/\lambda = 1.5\%$ and the intrinsic line width (standard deviation) of the Gaussian peak was set to $\sigma = 0.0500$ nm^{-1}. In order to elucidate how the peaks are affected as a function of their angular position, this calculation was done assuming various Bragg spacings. As can be seen, the broadening increases with increasing scattering vector. The figures given in the plot indicate the calculated standard deviation of the broadened Bragg peaks.

Desmearing procedures are discussed in references 2 and 3.

In summary, the bandwidth which is provided by the double multilayer monochromator is sufficient and suitable for
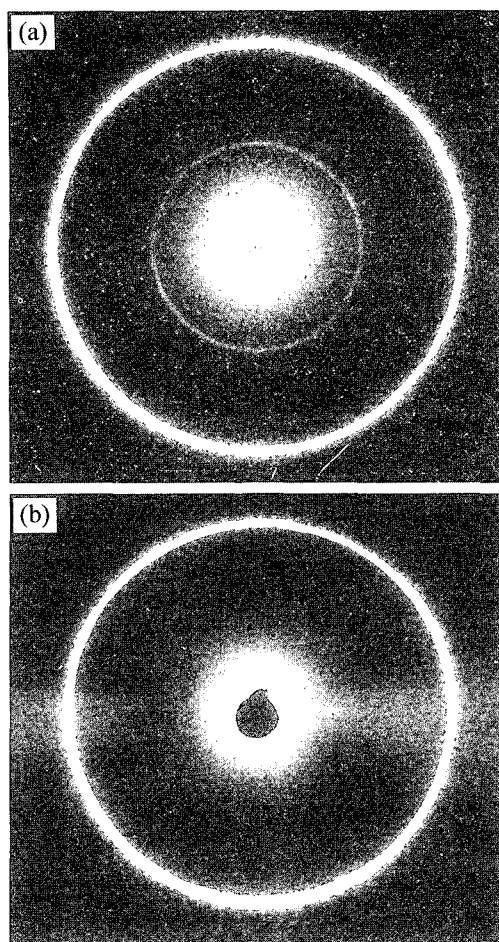
Figure 4. Diffraction pattern from lead stearate before (a) and after (b) a flat mirror had been installed. The weak diffraction ring in (a) corresponds to the diffraction of the second harmonic. It could be rejected upon reflecting the incident beam at the mirror surface.

most of the SAXS measurements which are typically performed at BL4C1 and no data correction procedures are required. In case of highly ordered samples, however, it is necessary to desmear the raw data, especially when intermediate or wide angles are being considered.

Mirror. In order to reject the higher harmonics from the beam which is reflected by the multilayer monochromator, a flat, gold-coated mirror (Beamline Technology Corp., USA) is installed 22 m from the source. The dimensions of the mirror are $200 \times 30 \times 30$ mm and the surface roughness is smaller than 1.5 Å. To prevent radiation damage on the mirror surface, it is kept in a box under a helium atmosphere. The tilt angle of the mirror is adjusted so that the beam is reflected under 8 mrad with respect to the mirror surface. At that angle the reflectivity for X-rays with $E = 7.7$ keV is about 75%, whereas it is less than 2% for the second harmonic. Thus, the total reflecting mirror acts as a low-pass

filter which effectively reduces the intensity of the second harmonic to a negligible level. The performance of the mirror is demonstrated in Figure 4. It compares the diffraction patterns from lead stearate which were measured by a charge-coupled device (CCD) detector before and after the installation of the mirror. Without the mirror, an intense diffraction ring was ob-served in the small-angle region, and in addition a weak ring at half angle. Upon installation of the mirror, only the intense diffraction ring remained. It is thus obvious that the weak ring must be attributed to the diffraction of the second harmonic, which could be effectively suppressed using the mirror.

Slit Collimation System. A very tight collimation of the X-ray beam and the minimization of any parasitic scattering is essential in small-angle scattering, so that measurements can be done in the immediate vicinity of the direct beam. Several slits are installed along the beam path for that purpose. A primary slit is located 14 m from the source point, in front of the monochromator. It is usually set to 0.5 mm vertically and 1.0 mm horizontally, thus slicing off a rectangular portion from the central cone of the emitted beam. The actual beam size is determined by two more slits behind the monochromator (one of those slits is scheduled to be installed in August 2001), whereas a guard slit just in front of the sample has the function to cut down any parasitic scattering without touching the main beam. This setting still needs to be optimized, because the parasitic scattering originating from the mirror cannot be completely removed with this configuration. Two viewing ports are installed along the beam path in order to monitor the shape and position of the X-ray beam.

SAXS Camera

The SAXS camera is enclosed in a safety hutch and all components are remotely controlled. A motorized sample stage is located 22.5 m from the source and allows users to install various sample cells in a flexible way. The photon flux at the sample position was estimated from the current measured with an ionization chamber to ca. 2×10^{10} photons/mm^2/s at a ring current of 200 mA. Attenuators with various thickness may be inserted into the beam in order to control the photon flux on the sample. An evacuated beam path with adjustable length (10, 90, 130, and 170 cm) is mounted on a double optical rail between the sample and the detector stage. It is sealed on both ends with thin Kapton foils and the vacuum level (typically 5×10^{-3} Torr) is continuously monitored. The beamstop, which is made of tantalium, is located inside the vacuum path, close to the Kapton window at the end. A motor-controlled detector stage is installed right behind the vacuum path. The intensity of the primary beam may be monitored by ionization chambers before and/ or behind the sample, and also by a scintillation counter which measures the back-scattering from the beamstop

under an angle of ca. 45°.

Detector Systems

At present two one-dimensional photodiode array detectors (PDA), an area-CCD detector, as well as phosphor imaging plates (IP) are available. In the following we will first discuss the properties, merits and demerits of each detector. Afterwards, we present SAXS measurements from some standard samples and compare the performance of the various detection systems.

Photodiode Array Detector System (PDA). This is an unintensified solid state detector which is based on an X-ray sensitive, linear silicon photodiode array (Princeton Instruments, USA, Model X/PDA). X-rays directly hit the sensing area after passing through the entrance window, which is made of beryllium. It is a multichannel line-scan camera which consists of two arrays placed one above the other. The total length of the combined arrays is two inches, which is divided into 2048 channels. The light sensing area per pixel is 25×25 μm^2. For storing the accumulated charge, however, a much larger area of 25×2500 μm^2 is used. This has an advantage that a high charge may be collected before the saturation level of a pixel is reached. Other merits of this type of integrating detector are its high gain (as compared to indirectly illuminated array detectors) and its high count rate capability, which is important when synchrotron radiation is used to measure intense diffraction peaks. According to the manufacturer, the spatial resolution is better than 1.5 pixels, geometric distortion less than one pixel and the uniformity of response is 5 to 10%. After a preset exposure time, the array is scanned and the charge in each diode is read out by the preamplifier board in the detector head. An analog signal is created and sent to the detector controller, where it is further shaped and amplified. It is then digitized by an analog-to-digital converter (ADC) with a resolution of 16 bit. The digitized signals are integer numbers measured in analog-to-digital units (ADU). They are sent via Direct Memory Access to the interface board of a personal computer, where data are displayed, further processed and stored.

A main disadvantage of this detector type is its inherently high dark current noise, which varies from pixel to pixel. Main sources of this background are thermally induced, statistical noise (accumulated charge in the array) as well as electronic noise originating from the readout electronics and from the digitizer. As thermally induced dark charge decreases exponentially with temperature, the array is cooled to typically -30°C. The thermoelectric cooler and the array are confined within a static vacuum chamber in order to prevent water condensation and to ensure optimal insulation. The detector is prone to radiation damage which is manifested in a locally increased dark current. Even though damaged areas may be recovered upon annealing the array, this process is not fully reversible. The dark current

increases linearly with the integration time, but in damaged pixels it increases much faster than in undamaged areas. The detector dark signal has to be determined carefully each time before a sample is to be measured. It has to be measured using the same integration time as for the sample and with the photon shutter being closed. The dark signal amounts to ca. 800 ADU when measured for 10 s. The detector is controlled using software provided by Princeton Instruments (Winspec 3.1) which automates data acquisition, display, and basic processing. Further data processing, as scaling, background subtraction and model fitting is done using other software developed by ourselves.

The linearity of the detector was checked by measuring the intensity of a Bragg peak from a block copolymer sample with ordered nano-domains as a function of the exposure time. The measured intensity shows good linearity with a relative error of less than 0.5%. It increases until the saturation level of the detector is reached (16 bit, or 65536 ADU). The dynamic range of the detector is greatly diminished due to the high dark signal, which has to be subtracted from the measured raw data. Thus, as shown in Figure 5, at long exposure times the maximum signal from the sample scattering does not reach the 16 bit level. It is reduced by the dark signal. In particular in case of weakly scattering samples, where long exposure times of several minutes are required for good counting statistics, the dark current may strongly dominate the measured raw data. In such a case the maximum exposure time is mainly determined by the accumulated dark current rather than by the scattering intensity
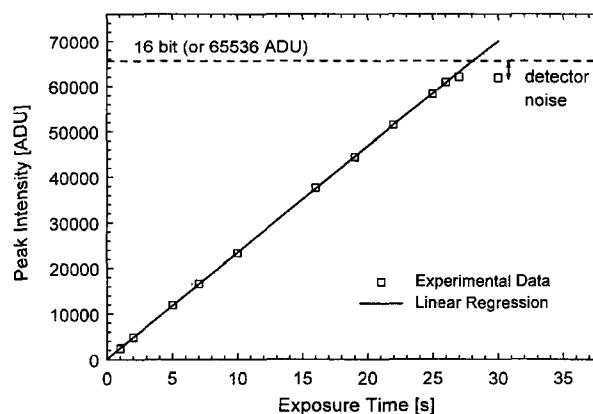

Figure 5. Measured diffraction peak intensity from an ordered block copolymer sample. Shown is the response of the PDA detector as a function of the exposure time. The full-well-capacity per pixel (i.e. the integrated signal which saturates a detector pixel) is 16 bit. Good linearity in the detector response was found until the pixel well capacity is reached. From the intensities which are displayed here, the dark noise was subtracted to yield solely the intensity scattered from the sample. Evidently, the dynamic range available for the sample is diminished due to the dark noise. This is becoming most severe when the scattering intensity from the sample under consideration is low.

of the sample. The PDA detector is not well-suited to study weakly scattering samples. Data then tend to become noisy after subtraction of the dark signal, because the dark signal itself shows a random fluctuation of ca. 0.5% when measured repeatedly.

Charge-Coupled Device (CCD) Area Detector. The unintensified CCD area detection system (Princeton Instruments, USA) is based on a scientific grade CCD image sensor (EEV 1152 × 1242 CCD, 1.4 Megapixel; EEV, U.K.), where charges are stored in an array of photo-sensitive capacitors. The entrance window of the detector is made of beryllium and has a diameter of 115 mm. Incident X-rays are converted by a 0.5 mm GdOs phosphor screen into visible scintillation photons which are guided to the CCD image sensor by a demagnifying fiber-optic taper with a reduction ratio of 4.6 : 1. The pixel size is $104 \times 104 \ \mu m^2$ at the entrance window and $22.5 \times 22.5 \ \mu m^2$ at the CCD image sensor. The sensor has a size of $25.9 \times 27.5 \ mm^2$ and is divided into 1152×1242 pixels. The diameter of the taper at the CCD is 25 mm. In order to reduce its dark current, the CCD is cooled to -50 °C by a Peltier device in combination with a circulating coolant. Water condensation inside the detector is prevented by evacuation. The output from the CCD is amplified, digitized by a 12- or 16-bit A/D converter, and transferred to the image memory of a Pentium computer via a high speed serial interface. Normal readout speed of the CCD at lowest noise is 200 KHz with a dynamic range of 16 bits per pixel. There also exists an option for a high speed readout at 1 MHz with a dynamic range of 12 bits per pixel. Other possibilities to achieve a faster readout are binning of pixels, partial readout, or a frame transfer mode. To prevent a smearing of the image during readout, an electromagnetic fast shutter, which is triggered by the detector controller, was installed close to the sample. The detector is controlled using software provided by Princeton Instruments (Winview32). It automates data acquisition, display, and basic processing. Further data processing, as e.g. circular averaging, scaling, background subtraction and model fitting is done using other software developed by ourselves.

As in case of the PDA detector, a precise measurement and subtraction of the dark charge signal is essential, in particular when low intensity patterns are to be measured. Compared to the PDA detector, the dark signal from the CCD is low and shows little fluctuation over the array. Fluctuations are further reduced upon circular averaging. When measured repeatedly, a stability of the dark signal within ca. 0.2% was found. The dark signal amounts to ca. 90 ADU within 1 s, most of which are offset counts from the A/D converter. Compared to the PDA detector, the CCD detector has only a very small increase of dark current with integration time, which makes it better suitable for measurements of samples with a low scattering intensity. According to the manufacturer the res-ponse nonuniformity is less than
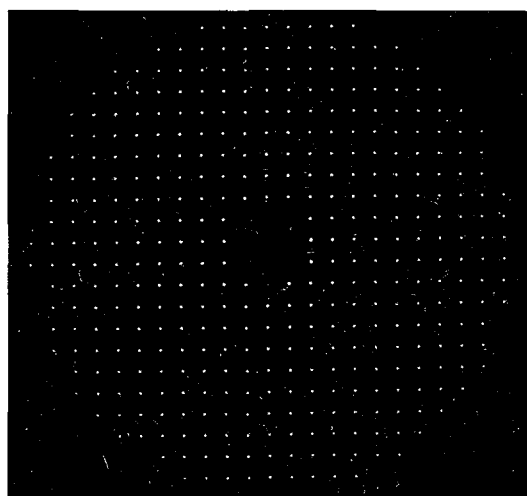

Figure 6. Image of a grid patterned mask measured with the CCD detector.

± 3% over the entire CCD area. The good linearity of the detector within the dynamic range was reconfirmed using the same method as for the PDA-detector (cf. Figure 5). The detector was checked for spatial distortion effects which could arise e.g. due to a shear distortion of the fiber optics taper. For that purpose the detector was illuminated through a grid patterned mask made of brass which consists of an array of holes 5 mm apart from each other with a hole diameter of 0.25 mm. The image ob-tained in that way (cf. Figure 6) is to be compared with the real geometry of the grid. We found a fairly good reproduction of the grid; the maximum deviation of a grid point from a straight line was found to be ca. 1% of the taper diameter at the CCD sensor side. Sophisticated software exists to correct acquired images for such spatial distortion effects.[12]

Phosphor Imaging Plate System. White image plates (Fuji BAS 2000) with a dimension of $400 \times 200 \ mm^2$ and a pixel size of $100 \times 100 \ \mu m^2$ are available. After exposure, the photo-stimulated phosphor screen is read out off-line with a MAC Science IPR-420 reader system and subsequently erased. The advantages of this integrating area detector are its high dynamic range (16 bit), a good detection quantum efficiency, and a very low readout or dark noise. On the other hand it is not well-suited for real time or time-resolved measurements.

First Experimental Results

Dried Polymer Latex. We now compare the performance of the various detector systems by discussing experimental data acquired from a polymer latex and from chicken tendon collagen. A latex, which is prepared by emulsion polymerization, consists of an aqueous dispersion of polymer particles with a particle size in the range of ca. 50-500 nm.[13] Here we discuss the scattering profiles obtained from highly
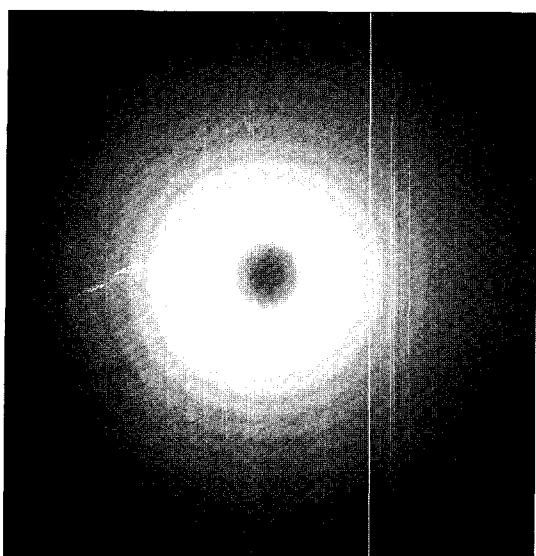
Figure 7. Scattering pattern of a PMMA latex powder acquired by the CCD detector with an exposure time of 2.5 s. The image is displayed on a logarithmic intensity scale in order to visualize the scattering features in the low intensity region more clearly.

uniform, spherical poly(methyl methacrylate) (PMMA) latex particles with a diameter of ca. 90 nm. The latex was dried at room temperature and subsequently ground to yield a fine powder. Even in the dried state, the spherical particles keep their identity due to the high glass transition temperature of PMMA.[14] We found that such a dried polymer latex is highly suitable to test critically the performance of detectors, because its scattering curve shows a number of peculiar characteristics: i) a very high scattering intensity, due to the high electron density contrast between the particles and the surrounding air, ii) a large number of oscillations due to the narrow particle size distribution and due to the symmetry of the particles, and iii) a steep, continuous decay of the intensity over several orders of magnitude within a small angular range. Thus, for the measurement of such a sample, a suitable detector is required to have a high count-rate capability, a good resolution, and a high dynamic range.

Figure 7 displays an image of the scattering pattern which was measured from the dried PMMA latex using the CCD detector system with an exposure time of 2.5 s. The intensity is displayed on a logarithmic scale for a better visualization of the data over the whole intensity range. Several rings of high and low intensity can be seen, due to the oscillations in the form factor of those uniform, spherical particles (cf. Figure 2). Furthermore it was found, that the scattering intensity of this sample is so high, that the contribution of any parasitic scattering to the measured intensity is negligible at all angles. As the sample under consideration is an isotropic powder, we will from now on discuss circularly averaged scattering profiles.

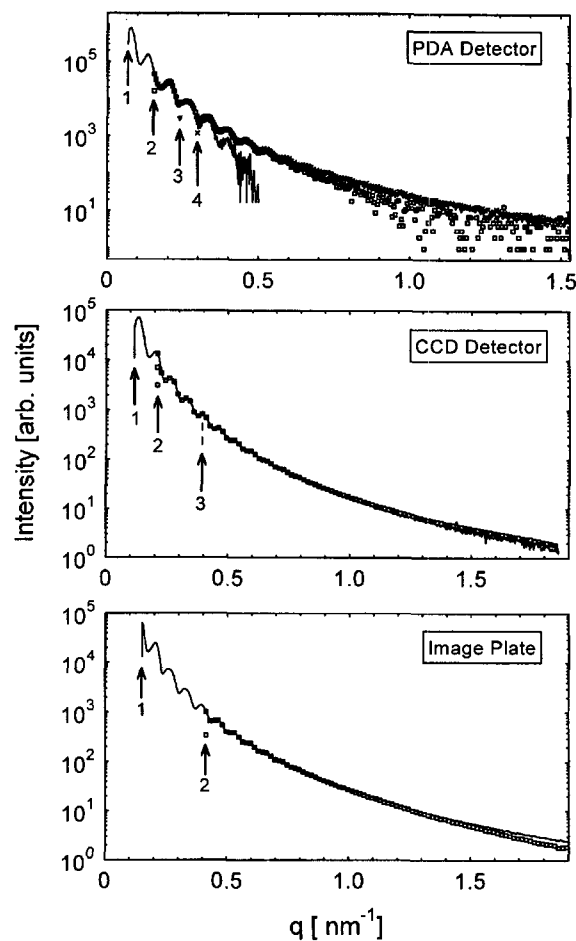Figure 8 displays the SAXS patterns of the dried PMMA

Figure 8. SAXS patterns from a dried PMMA latex measured with PDA and CCD detectors as well as with an image plate (IP). In order to check the dynamic range of the various detection systems the height (in case of the 1-D PDA detector) or diameter (in case of CCD area detector and IP) of the beamstop was varied and increasing parts of the highest intensity region were thus masked at smallest angles. The arrows indicate the first data point for the respective measurements.

latex measured with the PDA, CCD and image plate detection systems, respectively. In all cases, the sample-to-detector distance was ca. 110 cm. Following a procedure given by Fujisawa *et al.*,[15] the dynamic ranges of the detectors were checked by variation of the height (in case of the one-dimensional PDA detector) or diameter (in case of the CCD area detector and IP) of the beamstop, so as to mask increasing parts of the highest intensity region at small angles. In Figure 8 the first data points in the various measurements at different beamstop heights are marked by arrows and numbered consecutively. As can be seen from those data, the scattering intensity decays over nearly five orders of magnitude in the angular range under consideration and displays several maxima and minima at smallest angles.

In case of the PDA detector the decays of the curves

measured with various beamstop heights are clearly different. By using attenuators of various thickness it was found, that the shape and decay of the scattering pattern does not depend on the incident photon flux, even though the scattering intensity of this sample is very high. This shows that the detector has a high count rate capability and that the differences in the curves are due to the insufficient dynamic range of the detector. Using the PDA detector, it is not possible to measure simultaneously the regions of highest and lowest intensities correctly. The curves only superimpose when the beamstop is in positions numbered 3 and 4 in Figure 8. Thus, if such a sample is to be measured with the PDA detector, it is necessary to perform two measurements with the beamstop placed in positions 1 and 3, respectively. It is concluded that the practical dynamic range of this detector is limited to ca. 500 : 1.

In case of the CCD and IP detectors, the respective differences in the scattering curves acquired at various beamstop sizes are only marginal. This means that the dynamic range of those detectors is sufficient to simultaneously acquire data over an intensity range of at least 10^4: 1. Additional measurements using attenuators have shown, that both detectors are working correctly even at a very high count rates.

In Figure 9 the scattering data from the latex powder, which were acquired with the three different detectors, are shown together in a single plot. The displayed data for the PDA detector were combined from three measurements at different beamstop heights, whereas the data which are
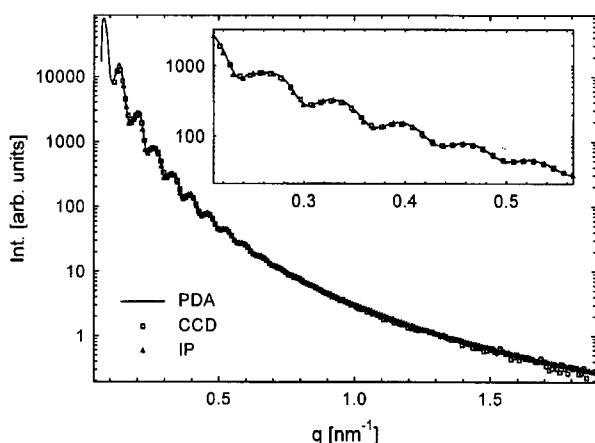
shown for the CCD and IP detectors are the single measurements at smallest beamstop size, respectively. As can be seen, all three curves superimpose very well at smallest angles where the oscillations appear, but also the decay of the intensity over more than four orders of magnitude is identical. In conclusion, when carefully applied, all available detectors can yield reliable SAXS data over a wide dynamic range and may reveal fine scattering features, provided that the scattering intensity from the sample is high.

Aqueous Polymer Dispersion. Next we discuss the performance of the detectors when samples with a lower scattering intensity are to be investigated. For that purpose an aqueous suspension of the PMMA latex was tested at a concentration of 17 vol%. In that case the scattering intensity is considerably lower than for the dried latex, because of the much lower electron density difference between PMMA and water, as compared to that between PMMA and air. To yield the scattering intensity from the latex particles only, it is necessary to measure separately the scattering from water and from the empty sample cell, and to subtract those contributions from the gross scattering curve measured from the aqueous dispersion, taking properly into account the respective transmission factors.[11] Figure 10 displays the thus obtained scattering curves which were acquired using the CCD detector and the imaging plate with an exposure time of 600 s. Like in the case of the latex powder sample, the data coincide well in the angular region of highest intensity where the oscillations occur. At higher angles ($q \geq$ 0.5 nm^{-1}), however, the CCD data become very noisy and at

Figure 9. Comparison of the SAXS patterns from a dried PMMA latex measured with the PDA and CCD detectors, as well as with an image plate (IP). The PDA data were combined from three measurements at three different beamstop heights (cf. Figure 8), whereas the CCD and IP data were collected in a single measurement using the smallest beamstop size. The inset shows a magnification of the curves in a small angular region. For sake of clarity, only every third measured data points are displayed for the CCD and IP detectors.
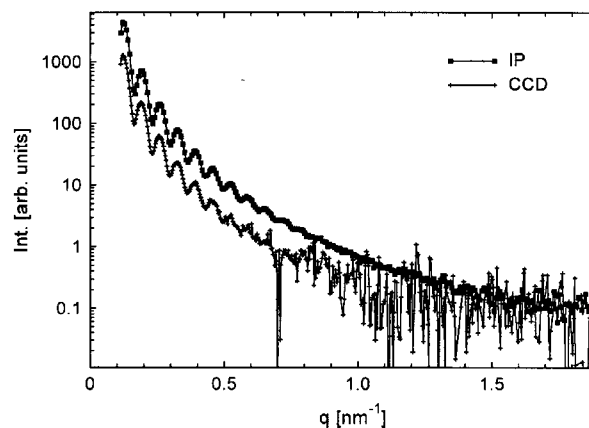

Figure 10. Comparison of the circularly averaged SAXS profiles from a PMMA latex dispersion (ca. 17 vol%) measured with the CCD detector and an image plate (IP), respectively. In both cases the data collection time was 600 s, the sample-to-detector distance was set to 110 cm and the beamsize at the sample position was ca. 0.40 × 0.20 mm^2. Note that the counting efficiency of the IP is approximately three times higher as compared to the CCD detector. The strong fluctuations of the CCD data at higher angles are mainly due to high contributions of dark and readout noise of the detector, which have to be subtracted.

scattering vectors higher than 1 nm^{-1} the data are no more meaningful. On the other hand, the data acquired with the image plate are smoother and show a reasonable decay in the whole angular range. The main reason for the strong noise in the CCD signal is the instability of its dark current. At high angles, the scattering intensity is considerably lower than the dark current, so that small fluctuations in the dark image can create a high noise level in the scattering curve, even if the data are circularly averaged. In case of the one-dimensional PDA detector this problem is even more severe, because the dark current is relatively much higher, especially when it is acquired over the period of a few minutes or longer. In addition, data smoothing by circular averaging is not applicable, of course. For the image plate system, dark and readout noise are negligible compared to the scattering intensity. The efficiency of the image plate is ca. 3.5 times higher as compared to the CCD. This is evident in Figure 10, where the measured scattering curves are displayed in the actual intensity ratio. This example has shown that among the currently available detector systems, the image plate is the detector of choice when weakly scattering samples are to be investigated.

It was possible to fit the experimental data from the PMMA latex using a model that assumes a system of homogeneous spheres with a mean diameter of 93.1 nm, and a standard deviation of the particle size distribution of 5.6%. The shape of the assumed particle size distribution function was slightly asymmetric.[11] Figure 11 shows that the data measured with the imaging plate are well fitted by such a model. In particular the oscillations and the overall decay are well matched. The scattering curve that we measured at BL4C1 also coincides very well with SAXS data which
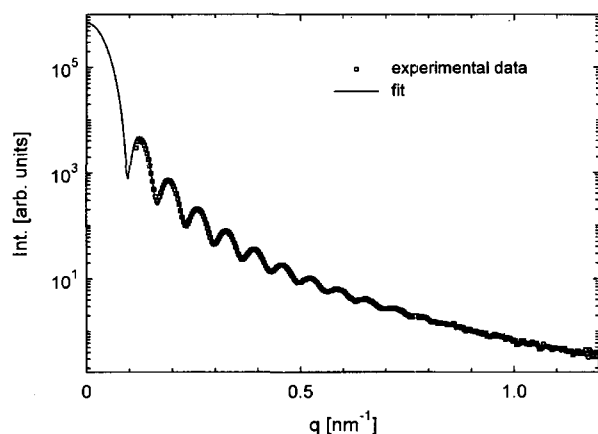
were acquired by others[16] from the same sample at the ESRF (European Synchrotron Radiation Facility, Grenoble, France).

Chicken Tendon Collagen. Figure 12 displays a small angle diffraction image which was acquired from a dry chicken tendon using the CCD detector with an exposure time of 100 s and a sample-to-detector distance of 110 cm. A large number of meridional reflections, which arise due to the periodic arrangement of collagen units along the fiber axis, could be detected. The repeat distance, which was obtained by using a PMMA latex of known particle size as a cross-calibrant, was determined to 643 Å. We observed a slow degradation of the collagen sample, so its repeat distance should be rechecked from time to time, if it is to be used as a SAXS calibrant. Figure 13 shows a one-dimensional slice of those diffraction data together with the diffraction pattern measured by the PDA detector. As can be seen, the patterns from both detector systems coincide well. In addition, the measured interpeak distances are highly periodic (cf. inset in Figure 13, which shows that both detectors are free from a significant spatial distortion. Together with other cross-calibrated samples (e.g. lead stearate, ordered block copolymer) the chicken tendon collagen is routinely used for angle calibration and for the exact determination of the center coordinates of the incident beam. Note that the measured higher order peaks in Figure 13 are considerably broadened, mainly due to the beam polychromaticity (cf. discussion of this point in connection with Figure 3). The first order Bragg peak of collagen could not be resol-ved at a camera length of 110 cm. Upon increasing the distance between sample and detector to 170 cm, the resolution of the SAXS camera can be increased to ca. 800 Å.
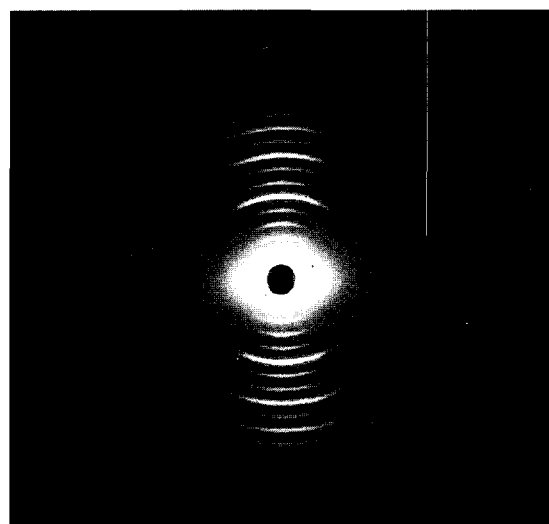

Figure 11. Circularly averaged SAXS data acquired from a PMMA latex (18 vol%) using an image plate detector. The exposure time was 600 s and the sample-to-detector distance was set to 110 cm. The experimental data were fitted with the scattering from a system of noninteracting, homogeneous spheres having an average diameter of 93.1 nm and a standard deviation of the (asymmetric) particle size distribution of 5.6%.

Figure 12. Diffraction pattern from a dry chicken tendon collagen acquired by the CCD detector with an exposure time of 100 s. The image is displayed on a logarithmic intensity scale in order to visualize the weaker diffraction peaks more clearly.
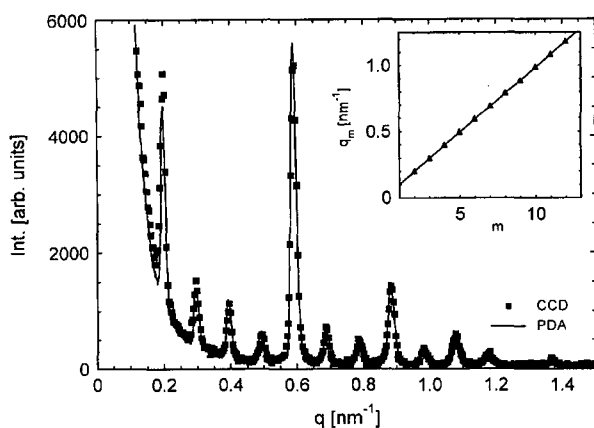
Figure 13. SAXS data measured from dried chicken tendon collagen using a CCD detector and a PDA detector at a sample-to-detector distance of 110 cm. The intensities were scaled with suitable factors to superimpose both curves, background scattering was not subtracted. The inset shows the position q_m of the Bragg peak maxima as a function of the order m of the peak. The slope of the linear fit curve is inversely proportional to the d-spacing.

Time-resolved SAXS Data. As an example for time-resolved SAXS measurements, Figure 14 displays experimental data acquired during the isothermal crystallization of a poly(ethylene tere-phthalate) sample.[17] Using a dual-chamber temperature jump unit, the sample was first molten at 280 °C in the upper chamber, and then rapidly transferred into another chamber (which is aligned in the X-ray beam), where the isothermal crystallization was carried out at 225 °C. Successive SAXS profiles were collected by the PDA detector with an acquisition time of 10 s per scan. During the induction period only diffuse scattering curves without maxima were observed. Above 90 s, a distinct scattering maximum appears. It progressively moves to higher scattering angles with time and simultaneously the integral scattering intensity (invariant Q) increases. The angle position of the broad diffraction peak is related to the average separation (long period L) of crystalline regions within a lamellar stack. Using a correlation function approach,[18] the change of morphological parameters (such as lamellar and amorphous layer thickness) could be extracted from the experimental data as a function of time.

Wide-angle Diffraction. Upon decreasing the sample-to-detector distance to ca. 10 cm, wide-angle diffraction (WAXD) measurements can be performed. As already discussed in connection with Figure 3, desmearing of the experimental data due to the wavelength spread in the incident beam is required when well-ordered samples are to be investigated. Corrections for the polarization factor and for smearing and distortion of the data due to the oblique incidence of the scattered beam on the flat detectors (because the solid angle subtended by one pixel on the detector changes with
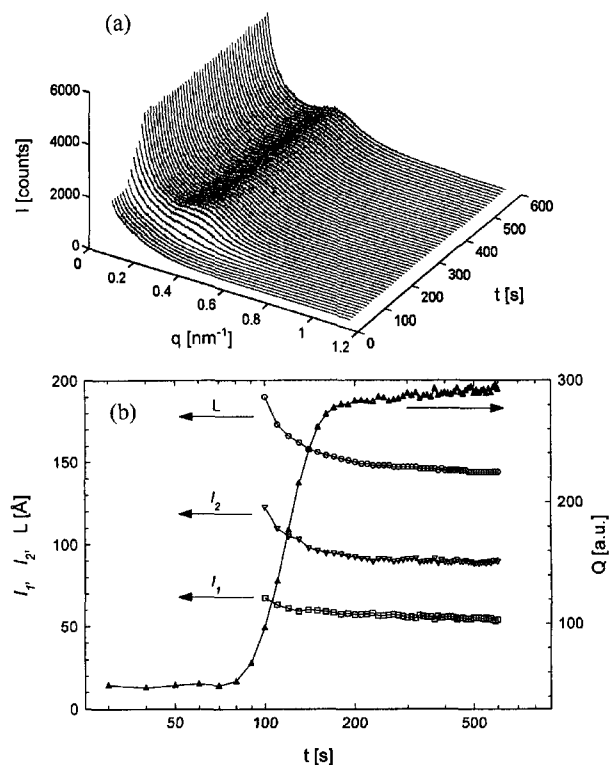

Figure 14. (a) Time-resolved SAXS patterns as collec-ted during the isothermal crystallization of PET at 225 °C. (b) Morphological parameters which were obtained from the data analysis: Long period L, lamellar thickness l_1, and amorphous layer thickness l_2. Q denotes the scattering invariant.

the scattering angle) are also required.[2,19,20] Furthermore, the $1/r^2$-dependence of the scattered intensity, as well as the angle-dependence of the absorption factor (inside the sample and between sample and detector) have to be considered. Note that all those points are of no concern for SAXS, due to the validity of small angle approximation in that regime. A typical application of WAXD which was performed at BL4C1 is the time-resolved study of the thermal imidization of a polyimide precursor to yield the corresponding polyimide.[21]

Outlook

In order to increase the photon flux at the sample position, a toroidal mirror will be installed at the beamline, using a 2 : 1 focusing geometry. Another slit will be added to further reduce the parasitic scattering at smallest angles. To increase the angle resolution, the maximum camera length will be extended to 3 m. Gabriel-type gas-filled proportional counters (1-D and 2-D) will be available for measuring samples with low scattering intensities. It is also planned to facilitate simultaneous SAXS/WAXD measurements. Absolute scattering intensities will be obtainable through cross-calibrated

standard samples.

References

(1) A. Guinier and G. Fournet, *Small Angle Scattering of X-rays*, Chapman & Hall, London, 1955.

(2) O. Glatter and O. Kratky, Eds., *Small Angle X-ray scattering*, Academic Press, London, 1982.

(3) L. A. Feigin and D. I. Svergun, *Structure Analysis by Small-angle X-ray and Neutron Scattering*, Plenum Press, New York, 1987.

(4) H. Brumberger, Ed., *Modern Aspects of Small-Angle Scattering*, Kluwer Academic Press, Dordrecht, 1995.

(5) R. J. Roe, *Methods of X-ray and Neutron Scattering in Polymer Science*, Oxford Univ. Press, Oxford, 2000.

(6) S. Doniach, *Chem. Rev.*, **101**, 1763 (2001).

(7) P. Cebe, B. S. Hsiao, and D. J. Lohse, Eds., *Scattering from Polymers: Characterization by X-rays, Neutrons and Light*, ACS Symposium Series 739, Oxford Univ. Press, 1999, and

(8) B. Chu and B. S. Hsiao, *Chem. Rev.*, **101**, 1727 (2001).

(9) T. -Y. Lee, J. Choi, Y. Chung, J. Y. Huang, J. M. Lee, S. H. Nam, and H. S. Youn, *Nuclear Instruments and Methods in Physics Research A*, **467-468**, 47 (2001).

(10) M. Ree, S. H. Woo, and T. J. Shin, *Polym. Sci. Technol. (Korea)*, **8**, 57 (1997).

(11) N. Dingenouts, J. Bolze, D. Pötschke, and M. Ballauff, *Adv. Polym. Sci.*, **144**, 1 (1999), and further references given therein.

(12) A. P. Hammersley, S. O. Svensson, A. Thompson, H. Graafsma, Å. Kvick, and J. Moy, *Rev. Sci Instr.*, **66**, 2729 (1995).

(13) R. G. Gilbert, *Emulsion Polymerization*, Academic Press, London, 1995.

(14) N. Dingenouts and M. Ballauff, *Langmuir*, **15**, 3283 (1999)

(15) T. Fujisawa, Y. Inoko, and N. Yagi, *J. Synchr. Rad.*, **6**, 1106 (1999).

(16) N. Dingenouts, *Röntgenkleinwinkelstreuung als Methodik der Strukturanalyse teilgeordneter Systeme*, Shaker Verlag, Aachen, 1999.

(17) S. W. Lee, B. Lee, and M. Ree, *Macromol. Phys. Chem.*, **201**, 453 (2000).

(18) G. R. Strobl and M. Schneider, *J. Polym. Sci.*, **18**, 1343 (1980).

(19) P. Norby, *J. Appl. Cryst.*, **30**, 21 (1997).

(20) M. Ree, S. H. Woo, K. Kim, H. Chang, W. C. Zin, K. -B. Lee, and Y. J. Park, *Macromol. Symp.*, **118**, 213 (1997).

(21) T. J. Shin, B. Lee, H. S. Youn, K. -B. Lee, and M. Ree, *Langmuir*, **17**, 7842 (2001).

further references given therein.